Biogeosciences
Discussions

Open Access

EGU

1 **Shift in the chemical composition of dissolved organic matter in the**

2 **Congo River network**

3 Thibault Lambert[1,*], Steven Bouillon[2], François Darchambeau[1], Philippe Massicotte[3],

4 and Alberto V. Borges[1]

5

6 [1] University of Liège, Chemical Oceanography Unit, Liège, Belgium

7 [2] K.U. Leuven, Department of Earth and Environmental Sciences, Leuven, Belgium

8 [3] Aarhus University, Department of Bioscience, Denmark

9 * Corresponding author

10

11

12

13

14

15 **Abstract**. The role of river ecosystems in processing inputs of dissolved organic matter

16 (DOM) from the terrestrial environment during downstream transport in river networks is

17 poorly constrained. In this study we report a data-set of DOM concentrations (dissolved

18 organic carbon) and composition (stable carbon isotopic composition, absorption and

19 fluorescence properties) acquired along a 1700 km stretch in the Congo River Basin, the

20 second river in the World. Samples were collected in the main river and its tributaries in

21 the central part of the Basin during high waters (HW) and falling waters (FW) periods. The

22    longitudinal increase in DOC concentrations and changes in DOM characteristics along

23    the mainstem was found to differ between the two periods, especially because of greater

24    photodegradation of terrestrial inputs from the DOM-rich waters from the Cuvette Centrale

25    during FW as water residence time (WRT) increased. DOM degradation within the Congo

26    Basin was found to result in the transition from aromatic to aliphatic DOM, resulting from

27    the losses of aromatic compounds by photodegradation and the production of aliphatic

28    compound by biological degradation. This study highlights that landscape properties and

29    changes in WRT can play a major role on the functioning of river ecosystems in processing

30    DOM during its downstream transformation in river networks.

31    **1. Introduction**

32    Dissolved organic matter (DOM) is composed of thousands of heterogeneous

33    compounds that differ in origin and reactivity (Leehneer and Croué, 2003) and is a central

34    component of the global carbon cycle (Battin et al., 2008). DOM in streams and rivers

35    mainly originates from the terrestrial ecosystem, but can also be fueled by internal sources

36    as stream order increases (Battin et al., 2008; Creed et al., 2015). Recent experimental

37    and field studies have evidenced that sorption, photochemical and biodegradation

38    processes continuously degrade and transform DOM throughout fluvial networks

39    (Massicotte and Frenette, 2011; Ward et al., 2013; Cory et al., 2014; Fasching et al., 2014;

40    Lapierre and del Giorgio, 2014). Large surveys of boreal lakes have suggested that DOM

41    was degraded along a gradient from aromatic to aliphatic compounds and that the

42    chemical properties of DOM pool were the dominant control of overall DOM reactivity

43    (Kothawala et al., 2014; Kellerman et al., 2015). Similarly, a large survey of temperate

44    streams and rivers have reported a preferential loss of aromatic DOM and parallel gain in

45    aliphatic DOM with increasing stream order, resulting in a diminution of the variability in

46    dissolved organic carbon (DOC) concentration and DOM composition from small

47    headwater streams to large rivers (Creed et al., 2015; see also Vannote et al., 1980).

48    However, the role of environmental factors (i.e. climatic variables, water chemistry,

49    landscape properties) on the DOM transformation in fluvial networks remains poorly

50    studied (Massicotte and Frenette, 2011; Marín-Spiotta et al., 2014; Creed et al., 2015).

51        The consideration of temporal dynamics in addition to the spatial dimension is

52    poorly investigated yet a crucial step towards a better understanding of DOM transport

53    and processing in fluvial networks. Temporal dynamics refer here to the changes of the

54    hydrological state of catchments that occur between high flow and low flow periods and

55    are susceptible to alter DOM dynamics for at least two reasons. First, the concentration,

56    the composition and the reactivity of DOM in streams and rivers are largely determined

57    by seasonal changes in water levels that control the hydrological connectivity between

58    fluvial networks and wetland sources (Besemer et al., 2009; Osburn et al., 2009; Bouillon

59    et al., 2012). Hydrological connectivity is particularly relevant regarding the role of fringing

60    wetlands that can regulate DOM inputs and composition along the river-floodplain

61    continuum (Junk et al., 1989; Battin, 1998; Cawley et al., 2012; Lambert et al., 2016).

62    Secondly, the increase in water discharge during high flow periods induces a decrease in

63    water residence time (WRT) within catchments due to increasing water velocities. Beyond

64    the role of external and intrinsic drivers on DOM degradation, WRT represents a major

65    control that regulates the degree of DOM transformation in aquatic ecosystems (Cory et

66    al., 2007; Battin et al., 2008; Weyhenmeyer et al., 2012; Lambert et al., 2016). According

67    to the recent pulse-shunt concept (Raymond et al., 2016) that builds on the "active pipe"

68    concept (Cole et al., 2007), the degree of DOM processing in fluvial networks should be

69    reduced during high flow periods as hydrological events favor the downstream DOM

70    transport through the drainage network and therefore reducing the time where dynamic

71    processes can take place.

72        African tropical rivers have among the highest specific flux of DOC worldwide

73    (Meybeck, 1993) and have an intense role in the global carbon cycle (Borges et al., 2015a;

74    2015b). Yet, they remain largely underrepresented in large-scale studies on DOM

75    processing (Lambert et al., 2015). The Congo is the largest river in Africa and the second

76    largest river in the world after the Amazon in terms of drainage basin area and water

77    discharge (Laraque et al., 2009). The Congo is also the second major exporter of

78    terrestrial organic carbon to the oceans after the Amazon, of which 85-90% being in the

79    form of DOC (Coynel et al., 2005), and drains the second largest tropical forested wetland

80    area, the Congolese 'Cuvette Centrale' (Bwangoy et al., 2010). Until now, the

81    biogeochemistry of DOM in the Congo and has been investigated in the Oubangui

82    catchment (Bouillon et al., 2014), in the western part of the basin (Mann et al., 2014),

83    along the 350 km final stretch of the river to the head of its estuary (Spencer et al., 2012),

84    and in a small catchment (Epulu River) on the Eastern part of the basin (Spencer et al.

85    2010). Downstream gradient of DOM in the mainstem of the Congo is thus poorly

86    constrained in its central part, where the river drains the Cuvette Centrale and receives

87    inputs from its major tributaries (Fig. 1).

88        Emerging concepts aiming to describe how inland waters transform DOM flowing

89    down the river continuum, namely the "chemostat" hypothesis (Creed et al., 2015) and the

90    pulse-shunt concept (Raymond et al., 2016), need to be tested to extensive field studies

91    in tropical ecosystems. Indeed, ~60% of the global riverine C transport is thought to occur

92    in the tropical zone (Ludwig et al. 1996). The Congo mainstem and its tributaries were

93    sampled along a 1700 km stretch from the city of Kisangani to the city of Kinshasa during

94    two contrasted hydrological periods (Fig. 1 and 2). DOM was characterized through its

95    optical properties, its stable carbon isotope composition ($\delta^{13}C_{DOC}$) and its content in DOC.

96    Optical measurements (including absorption and fluorescence) have been underscored

97    as an efficient tool for the characterization of the chemical structure and reactivity of DOM

98    at large spatial scales (Massicotte and Frenette, 2011, Cawley et al., 2012; Kothawala et

99    al., 2014; Lambert et al., 2016), notably with the development of multicomponent

100   deconvolution techniques such as the parallel factor analysis (PARAFAC) (Stedmon et

101   al., 2003; Murphy et al., 2013). The aim of this study was to (1) characterize the

102   longitudinal evolution of DOM in the Congo River during its passage through the Cuvette

103   Centrale and (2) investigate the role of environmental drivers and WRT on DOM

104   processing across a gradient of streams and rivers in the second largest river in the tropics

105   and in the World.

106   **2. Material and Methods**

107   **2.1 Study site.**

108       The Congo is the largest river in Africa and the second largest river in the world

109   after the Amazon in terms of drainage basin area (~3.7 x $10^6$ km²) and water discharge

110   (~43 000 m³ s⁻¹) (Laraque et al., 2009). The river originates in the southeastern part of the

111   basin, and is called the Lualaba until it crosses the city of Kisangani and becomes officially

112   known as the Congo. The Congo basin straddles on the equator, with major tributaries

113   located on both hemispheres (Fig. 1). Thus, the rainy season on the northern part of the

114   basin is compensated by the dry season on the southern part of the basin, and *vice-versa*,

115   leading to an attenuation of seasonal water height variations (Runge, 2008), in stark

116    contrast with the Amazon river, leading to marked differences in biogeochemistry (e.g.

117    $CH_4$ dynamics, Borges et al. 2015b) and aquatic ecology (e.g. phytoplankton

118    development, Descy et al. 2016) between these two rivers. The hydrological cycle of the

119    Congo is bimodal, with maximum water flow occurring in December and May and

120    minimum flow in August and March (Fig. 2). The center of the basin is covered by

121    evergreen forest (~50% of the total area), and surrounded by savannah in the northern

122    and southern rims of the catchment. The Cuvette Centrale is located in the central part of

123    the basin on both side of the equator and consists mainly in a vast permanently flooded

124    forested area of $360 \times 10^3$ km² (Bwangoy et al., 2010). The core of the Cuvette Centrale

125    corresponds to a net increase in the wetland fraction along the Congo River as the

126    mainstem connects with large tributaries flowing through the flooded forest (Fig. 1 and

127    Supplementary Fig. 1). The most important tributaries of the Congo in terms of discharge

128    are the Oubangui (4200 $m^3$ $s^{-1}$) and the Sangha (2220 $m^3$ $s^{-1}$) on the northern side, the

129    Kasai (9000 $m^3$ $s^{-1}$) on the southern side, and the Ruki (3950 $m^3$ $s^{-1}$) and the Lulonga

130    (2040 $m^3$ $s^{-1}$) along the equator (Bricquet, 1995; Coynel et al., 2005; Laraque et al., 2009).

131    **2.2. Field data collection.**

132    Samples were collected during the yearly discharge maximum in December (03-19

133    December 2013) and during falling waters following the second discharge maximum

134    occurring in March (10-30 June 2014) (Fig. 2). The sampling concerned the Congo River

135    itself as well as its small and large tributaries (Table 1). Stations along the mainstem were

136    located ~50 km apart from Kisangani to Kinshasa. Major tributaries included the Tshopo,

137    the Lindi, the Itimbiri, the Aruwini, the Mongala, the Oubangui, the Sangha and the Lefini

138    on the right side of the Congo, and the Lomami, the Lulonga, the Ikelemba, the Ruki and

139　the Kwa/Kasai on the left side. The Lefini was sampled only during the first campaign

140　(high waters).

141　　　　Water sampling was performed from a 22 m boat on the mainstem and with a canoe

142　in the tributaries. Approximately 2 L of water were collected 0.5 m below the surface, kept

143　away from direct sunshine and filtered and conditioned typically within 15 min of sampling.

144　Filtrations were performed successively on pre-combusted GF/F glass fiber filters (0.7 µm

145　porosity), then on 0.2 µm polyethersulfone syringe filters. Samples for the measurement

146　of DOC concentration and $\delta^{13}C_{DOC}$ signatures were stored in 40 mL glass vials with

147　polytetrafluoroethylene (PTFE) coated septa with 50 µL $H_3PO_4$ (85%). Samples for

148　colored DOM (CDOM) and fluorescent DOM (FDOM) analyses were stored in 20 mL

149　amber glass vials with PTFE-coated septa but without $H_3PO_4$ addition. Samples for major

150　elements (including Fe) were stored in 20 mL scintillation vials and acidified with 50 µl of

151　$HNO_3$ 65 % prior to analysis.

152　　　　Fe was measured by inductively coupled plasma spectrometry (Agilent 7700x ICP-

153　MS). DOC and $\delta^{13}C_{DOC}$ were analyzed with an Aurora1030 total organic carbon analyzer

154　(OI Analytical) coupled to a Delta V Advantage isotope ratio mass spectrometer. Typical

155　precision observed in duplicate samples was in >95% cases < ± 5 % for DOC, and ± 0.2

156　‰ for $\delta^{13}C_{DOC}$. Quantification and calibration was performed with series of standards

157　prepared in different concentrations, using both IAEA-C6 ($\delta^{13}C$ = -10.4 ‰) and in-house

158　sucrose standards ($\delta^{13}C$=-26.9 ‰). All data are reported in the δ notation relative to VPDB

159　(Vienna Pee Dee Belemnite). Absorbance was recorded on a Perkin-Elmer UV/Vis 650S

160　spectrophotometer using a 1 cm quartz cuvette. Absorbance spectra were measured

161　between 200 and 700 nm at 1 nm increment and instrument noise was assessed

162　measuring ultrapure (Type 1) Milli-Q (Millipore) water as blank. After subtracting the blank

163   spectrum, the correction for scattering and index of refraction was performed by fitting the

164   absorbance spectra to the data over the 200-700 nm range according to the following

165   equation:

166   $$A_\lambda = A_0 e^{-S(\lambda - \lambda_0)} + K \qquad\qquad (1)$$

167   where $A_\lambda$ and $A_0$ are the absorbance measured at defined wavelength λ and at reference

168   wavelength $\lambda_0$ = 375 nm, respectively, S the spectral slope ($nm^{-1}$) that describes the

169   approximate exponential decline in absorption with increasing wavelength and K a

170   background offset. The fit was not used for any purpose other than to provide an offset

171   value K that was then subtracted from the whole spectrum (Lambert et al., 2015).

172   Fluorescence intensity was recorded on a Perkin-Elmer LS45 fluorescence spectrometer

173   using a 1 cm quartz cuvette across excitation wavelengths of 220-450 nm (5 nm

174   increments) and emission wavelengths of 230-600 nm (0.5 nm increments) in order to

175   build excitation–emission matrices (EEMs). If necessary, samples were diluted until $A_{254}$

176   < 0.2 $m^{-1}$ to avoid problematic inner filter effects (Ohno, 2002). Before each measurement

177   session (i.e. each day), a Milli-Q water sample was also measured and subtracted from

178   EEMs.

179   Water temperature, %$O_2$, and pH were measured *in situ* with portable field probes

180   calibrated using standard protocols (YSI ProPlus probe). Pelagic respiration (R) was

181   determined from the decrease of $O_2$ in 60 ml biological oxygen demand bottles over ~24

182   h incubation periods. The bottles were kept in the dark and close to in situ temperature in

183   a cool box filled with in situ water. The $O_2$ decrease was determined from triplicate

184   measurements at the start and the end of the incubation with an optical $O_2$ probe (YSI

185   ProODO). The respiratory quotient (RQ) is defined as the molar ratio of $O_2$ consumed to

186    $CO_2$ produced by respiration, and allows the conversion of respiration measurements from

187    $O_2$ to C units. The RQ value is in theory equal to 1 for the oxidation of glucose, but higher

188    than 1 for more complex and reduced organic molecules containing nitrogen and

189    phosphorous, such as lipids and proteins (e.g. 1.3 in a temperate stream with a catchment

190    dominated by pastures (Richardson et al., 2013), or lower than 1 for highly oxidized and

191    oxygen-rich molecules (e.g. pyruvic, citric, tartaric, and oxalic acids) (e.g. 0.8 in boreal

192    lakes, Berggren et al. 2012). Given the range of RQ values, we adopted a RQ value of

193    1.0. The vertical light attenuation coefficient, $K_d$ ($m^{-1}$), was calculated from simultaneous

194    measurements of surface irradiance with a Li-Cor LI-190 quantum sensor and underwater

195    photosynthetically active radiation (PAR) measurements with a submersible Li-Cor LI-

196    193SA spherical quantum sensor. $K_d$ was derived from the slope of the semi-logarithmic

197    regression between relative quantum irradiance and depth. Transparency of water column

198    was measured using a 20-cm diameter Secchi disk.

199    **2.3. Characterization of DOM composition.**

200    The specific ultra-violet absorbance ($SUVA_{254}$) was calculated as the UV

201    absorbance at $\lambda$ = 254 nm ($A_{254}$) normalized to the corresponding DOC concentration

202    (Weishaar et al., 2003). The natural UV absorbance of Fe at $\lambda$ = 254 nm was estimated

203    based on measured Fe concentrations and was then subtracted from the UV absorbance

204    measured. The corrected value of $A_{254}$ was then used to calculate $SUVA_{254}$. The $SUVA_{254}$

205    was used as an indicator of the aromaticity of DOC with high values (>3.5 l $mgC^{-1}$ $m^{-1}$)

206    indicating the presence of more complex aromatic moieties and low values (<3 l $mgC^{-1}$ $m^{-1}$)

207    $^{1}$) indicative the presence of mainly hydrophobic compounds (Weishaar et al., 2003).

208    Napierian absorption coefficients were calculated according to:

209    $a_\lambda = 2.303 \times A_\lambda/L$                    (2)

210    where $a_\lambda$ is the absorption coefficient (m$^{-1}$) at wavelength $\lambda$, $A_\lambda$ the absorbance corrected

211    at wavelength $\lambda$ and L the path length of the optical cell in m (0.01 m). CDOM was reported

212    as the absorption coefficient at 350 nm ($a_{350}$). Spectral slopes for the intervals 275-295

213    ($S_{275\text{-}295}$) nm and 350-400 nm ($S_{350\text{-}400}$) were determined from the linear regression of the

214    log-transformed $a$ spectra versus wavelength. The slope ratio $S_R$ was calculated as the

215    ratio of $S_{275\text{-}295}$ to $S_{350\text{-}400}$ (Helms et al. 2008). $S_R$ is related to the molecular weight (MW)

216    distribution of DOM with values less than 1 indicative of enrichment in high molecular

217    weight compounds and high values above 1 indicative of a high degree of low molecular

218    weight compounds. The fluorescence index (FI) was calculated as the ratio of the

219    emission intensities at 470 nm and 520 nm at an excitation wavelength of 370 nm

220    (McKnight et al., 2001). A higher FI value (e.g., 1.8) indicates an aquatic microbial DOM

221    source while a lower value (e.g., 1.2) indicates a terrestrial source. Intermediate values

222    indicate a mixed DOM source.

223    **2.4. PARAFAC modeling.**

224    EEMs preprocessing steps (removing first and second Raman scattering,

225    standardization to Raman units, absorbance corrections and inner filter effects) wwereas

226    performed prior the PARAFAC modeling. The scans were standardized to Raman units

227    (normalized to the integral of the Raman signal between 390 nm and 410 nm in emission

228    at a fixed excitation of 350 nm) with a Milli-Q water sample run the same day as the

229    samples (Zepp et al., 2004). PARAFAC model was build using MATLAB (MathWorks,

230    Natick, MA, USA) and the drEEM Toolbox version 1.0 (Murphy et al., 2013). Validation of

231    the model using normalized EEMs was performed through by split-half analysis and

232    random initialization. The normalization step was applied to scale each EEM to its total

233    signal, thus ensuring the model focused entirely on compositional rather than

234    concentration gradients. Additional samples analyzed in the same manner and collected

235    from the Kwa/Kasai river basin ($n$ = 104), Lago Janauacá (a central Amazon floodplain

236    lake, $n$ = 17), the Niger River ($n$ = 19) and the Okavango delta were added to the dataset

237    to increase the variability of DOM fluorescence signatures and help detect components

238    that could have been present in insufficient quantity to be detected in our environment.

239    The maximum fluorescence $F_{Max}$ values of each component for a particular sample

240    provided by the model were summed to calculate the total fluorescence signal $F_{Tot}$ of the

241    sample in Raman unit (R.U.). The relative abundance of any particular PARAFAC

242    component X was then calculated as $\%C_X = F_{Max}(X)/ F_{Tot}$.

243        The positions of maximum peaks established by our model were compared to the

244    classical excitation-emission matrices nomenclatures (Fellman et al., 2010; Coble et al.,

245    2014) and with other reported PARAFAC models built in a large variety of freshwater

246    ecosystems (Table 2). Additionally, each PARAFAC component was associated to a

247    dominant molecular class based on recent studies aiming to correlate individual molecular

248    formula with different PARAFAC components through Fourier transform ion cyclotron

249    resonance mass spectrometry (FTICR-MS). Such studies have been carried out in high

250    latitude lakes (Kellerman et al., 2015), boreal rivers (Stubbins et al., 2014) and subtropical

251    wetland (Wagner et al., 2015). Although such comparison has not be carried out with our

252    own samples, the relatively good consistency of associations between optical and

253    molecular linkages observed in contrasting environments suggests that PARAFAC

254    components can track dominant DOM molecular composition similarly across different

255    biomes in terms of DOM MW and enrichment in aliphatic or aromatic molecules (Wagner

256    et al., 2015).

257    **2.5. Landscape analysis.**

258    The total drainage area and the Strahler stream order (Strahler, 1957) were

259    calculated at each station in the geographic information system (GIS) software ArcGis®

260    (ESRI 2011, ArcGis Desktop 10.3.1), using the ArcHydro tools (v. 2.0) and the

261    hydrological data and maps based on shuttle elevation derivatives at a 3" resolution

262    (Lehner et al., 2008). The extent of wetland areas and dense forest cover were extracted

263    from the Global Lakes and Wetlands Database (Lehner and Döll, 2004) and from Global

264    Land Cover 2009 database (Bontemps et al. 2011), respectively.

265    **2.6 Statistical Analysis.**

266    Mann-Whitney t-tests were performed to investigate the difference in DOM

267    properties spatially (mainstem *versus* tributaries) and temporally (HW *versus* FW). A

268    principal component analysis (PCA) was also performed to explore DOM evolution during

269    its transport through the Congo fluvial network. The optical properties of DOM including

270    level of CDOM ($a_{350}$), bulk composition ($SUVA_{254}$, $S_R$, FI) and the relative abundance of

271    PARAFAC components were used as the variables. Given the different units of these

272    variables, data were scaled to zero-mean and unit-variance as recommended (Borcard et

273    al., 2011). The PCA was performed using the prcomp function in R software.

274    **3. Results**

275    **3.1. DOM concentration and bulk composition.**

276    DOC concentrations in the mainstem were higher during HW (5.4 – 13.9 mg L$^{-1}$,

277    average 8.2±2.6 mg L$^{-1}$) compared to FW (4.2 – 9.8 mg L$^{-1}$, average 5.9±1.8 mg L$^{-1}$) but

278    showed similar longitudinal trends during both hydrological periods (Fig. 3a, 3b): DOC

279    increased slowly in the upper part of the transect and then faster as the Congo River

280    evolves throughout the core of the Cuvette Centrale and mixes with the Kwa/Kasai River

281 (Fig. 1). The breaking point of in the DOC longitudinal evolution increase in DOC

282 concentrations is located at km 700 during HW, and around km 500 during FW. DOC in

283 tributaries were highly variable (from 1.8 to 67.8 mg $L^{-1}$) and were found to be correlated

284 with the extent of flooded forest (Fig. 4), resulting in highest concentrations in tributaries

285 draining the Cuvette Centrale and lowest concentrations in those draining savannah areas

286 upstream of Kinshasa (Fig. 1). Tributaries located downstream of the Cuvette Centrale

287 were also characterized by lowest DOC concentrations during FW compared to HW while

288 no clear pattern was observed for those located upstream.

289 $\delta^{13}C_{DOC}$ signatures in the mainstem were lower during HW (from 30.6 to -28.8 ‰,

290 average -29.4±0.3 ‰, $n$ = 35) compared to FW (from -29.3 to -25.2 ‰, average -27.5±0.9

291 ‰, $n$ = 34). $\delta^{13}C_{DOC}$ during HW decreased about 0.7 ‰ from Kisangani to km ~ 1200,

292 remained stable until km ~ 600 and then increased slightly towards Kinshasa. During FW,

293 $\delta^{13}C_{DOC}$ decreased markedly about 3 ‰ between Kisangani and km ~ 1600. Downstream,

294 values were variable (-27.2±0.6 ‰ between km 600 – 1600, $n$ = 18) and then showed ~ 1

295 ‰ drops at km ~ 600 and ~ 200, coinciding with the confluence zones with the Oubangui

296 and the Kwa/Kasai rivers, respectively. In tributaries, $\delta^{13}C_{DOC}$ values displayed a similar

297 pattern during the two hydrological periods with lowest and relatively stable values (-

298 29.7±0.5 ‰, $n$ = 76) in streams and rivers draining dense forest areas and higher

299 signatures in those flowing savannah areas 0-400 km upstream of Kinshasa (-28.1±0.8,

300 n = 14). Stations of the mainstem located within or upstream the Cuvette Centrale were

301 characterized by highest $\delta^{13}C_{DOC}$ values than those measured in tributaries collected

302 along the same transect, both during HW ($p < 0.004$) and FW ($p < 0.0001$). Downstream

303 the Cuvette Centrale, stations of the mainstem had lower $\delta^{13}C_{DOC}$ signatures than those

304 measured in tributaries ($p < 0.0001$, all periods).

305    SUVA$_{254}$ and S$_R$ during the two hydrological periods varied mainly between 4.0 –

306    5.2 L mgC$^{-1}$ m$^{-1}$ and 0.734 – 0.802 among all stations, respectively (10% – 90%

307    percentiles, n=160), indicating that DOM in the Congo basin was dominated by aromatic

308    compounds of high MW during both periods (Fig. 3e-3h). SUVA$_{254}$ generally decreased

309    from Kisangani to Kinshasa in the mainstem during HW, with a slight increase between

310    km 500 and 800 upstream of Kinshasa, while S$_R$ exhibited stable values from Kisangani

311    and then started to increase toward Kinshasa at km 700. Compared to HW, SUVA$_{254}$

312    during FW was relatively stable and lowest from Kisangani to km 500 but higher between

313    km 0 – 500 as SUVA$_{254}$ increased markedly in this section (p < 0.0001). S$_R$ exhibited a

314    hump-shaped pattern during FW, with increasing values from Kisangani to km 500 and

315    decreasing value between km 0 – 500. A slight decrease in SUVA$_{254}$ (p = 0.0043)

316    associated with an increase in S$_R$ (p = 0.047) was also observed between km 200 – 400.

317    Generally, SUVA$_{254}$ in tributaries were slightly higher in FW than at HW (p = 0.035), similar

318    to the mainstem in HW but higher in FW (p = 0.0113). FI in the mainstem gradually

319    decreased from Kisangani to Kinshasa during both hydrological periods, with higher

320    values during FW than in HW (p = 0.0006), but were generally highest than in tributaries

321    (p < 0.0001). No distinct seasonal variation was apparent in tributaries.

**322    3.2. PARAFAC results.**

323    Six PARAFAC components were determined to adequately model our dataset

324    (Table 2, Supplementary Fig. 2). Components C1, C3, C4, and C5 are all classified as

325    "humic-like" but have been shown to differ in terms of sources, molecular association and

326    reactivity (Table 2). C1 and C3 are commonly reported in freshwaters ecosystems and

327    are associated with a group of high MW and aromatic molecules of terrestrial origin (e.g.

328    Wagner et al., 2015). Both are susceptible to photodegradation (Lapierre and del Giorgio,

329    2014). C4 is associated with terrigenous molecules of lower aromaticity and MW relative

330    to C1 and C3 (Kellerman et al., 2015). In freshwaters, C4 can originate from terrestrial

331    inputs (Stedmon and Markager, 2005; Yamashita et al., 2010), especially from wetland

332    areas (Lambert et al., 2016), but can also be produced by photodegradation of terrestrial

333    organic matter (Massicotte and Frenette, 2010). Among the humic-like compounds, C5 is

334    associated with molecules characterized by lowest aromaticity and MW (Stubbins et al.,

335    2014) and has been found to be a photoproduct derived from terrestrial DOM (Lapierre

336    and del Giorgio, 2014). C2 and C6 are respectively classified as microbial humic-like and

337    tryptophan-like component (Fellman et al., 2010). By opposition to the other components,

338    C2 and C6 are associated with low MW DOM fractions enriched in aliphatic molecules

339    biologically produced within aquatic ecosystems (Kellerman et al., 2015; Wagner et al.,

340    2015). Both C2 and C6 can be assigned to fraction of DOM resulting from the microbial

341    degradation of terrestrial organic matter within freshwaters (Stedmon et al., 2003; Walker

342    et al., 2013), although autochthonous primary production represents another potential

343    source for C6 (Yamashita et al., 2010).

344         The relative contribution of C1 and C3 showed similar patterns along the mainstem

345    during both hydrological periods (Fig. 5). %C1 and %C3 presented a slight decrease then

346    increased during HW with minimal contribution recorded around km 1100. %C1 and %C3

347    were lowest during FW ($p$ = 0. 017 and $p$ < 0.0001, respectively), with low variability

348    upstream of km 500 and highest contribution downstream. %C4 displayed a general

349    increase along the transect at HW especially marked between Kisangani and km ~1100

350    and between km 600 to km 150. During FW, %C4 was opposite to the longitudinal

351    evolution of %C1 and %C3, with highest contribution than during HW ($p$ > 0.0001). Overall,

352    %C5 was higher during FW than during HW ($p$ < 0.0001) and exhibited longitudinal

353    patterns opposite to those of %C3 during both periods. %C2 was relatively stable along

354    the mainstem during both periods, with higher contribution during FW compared to HW (p

355    = 0.0076). C6 exhibited the lowest contribution to FDOM signal and %C6 trended to be

356    lower during FW compared to HW. Longitudinal evolution of C6 was characterized by a

357    strong drop along the mainstem, occurring around km 800 at HW and km 500 at FW.

358        Overall, tributaries were characterized by lower %C2, %C3 and %C6 relative to the

359    mainstem (p < 0.0001). %C4 and %C1 were respectively higher (p = 0.0007) and lower

360    (p = 0.017) in tributaries than in the mainstem during HW, and no difference was observed

361    at FW. No difference was observed for %C5 between tributaries and the mainstem for

362    both periods. The seasonal variability within tributaries was characterized by higher

363    contribution of C4 (p = 0.025) and C5 (p < 0.0001) and lower contribution of C3 (p =

364    0.0015) and C6 (p = 0.003) in FW compared to HW.

365    **3.3. PCA results.**

366        The first two principal component (PC) accounted for 57% of the total variance (Fig.

367    6). The first PC (PC1) showed a transition from terrestrial aromatic DOM (%C3, SUVA$_{254}$,

368    DOC, a$_{350}$, positive loadings) to aliphatic DOM (%C2, %C6, FI, negative loadings). The

369    second PC (PC2) suggests a transition from highly aromatic terrestrial DOM (%C1, %C3

370    and SUVA$_{254}$, negative loadings) to DOM of lower aromaticity and MH (%C4, %C5, S$_{R}$,

371    positive loadings). The distribution of sampling stations for a given Strahler order was

372    highly heterogeneous (Fig. 6a). However, a global pattern emerges along PC1 with

373    stations collected in the mainstem showing mainly negative scores (Fig. 6b). Furthermore,

374    stations of the mainstem collected during HW had negative scores along PC2, but positive

375 scores during FW. Overall, stations collected during HW had mainly negative scores along

376 PC2 while those sampled at FW showed large variability along PC2.

377 **4. Discussion**

378 **4.1. Longitudinal evolution of DOM in the Congo River**. The Congo River from

379 Kisangani to Kinshasa continually receives organic matter inputs from inflowing tributaries

380 enriched in DOM from the flooded forest (Fig. 4), resulting in a net increase in DOC

381 concentrations along the longitudinal axis during both periods. Our data showed however

382 that the longitudinal evolution in DOM content and composition differed between the two

383 campaigns. These differences result from the combination of several factors.

384 **4.1.1. Seasonal changes in DOM sources mobilized in the upper basin.** The large

385 variation in $\delta^{13}C_{DOC}$ values in the mainstem at Kisangani between HW (-29.0 ‰) and FW

386 (-25.2 ‰) can be related to a shift in the source of DOM mobilized in the upper part of the

387 basin due to differences in water routing during the hydrograph. Thus, decreasing $\delta^{13}C_{DOC}$

388 signatures that occurred with increasing water discharge during high flow periods has

389 been attributed to the mobilization of fresh DOM from superficial soil horizons in wide

390 variety of catchments (Neff et al., 2006; Sanderman et al., 2009; Lambert et al., 2011;

391 Bouillon et al., 2012). Inversely, highest $\delta^{13}C_{DOC}$ values during low flow periods reflect the

392 deepening of water flow paths and the subsequent mobilization of more degraded DOM

393 from deeper soil horizons. This seasonal change in DOM composition at the start of the

394 Kisangani – Kinshasa transect are further supported by an ongoing high frequency

395 monitoring carried out à Kisangani (unpublished data).

396 **4.1.2. Impact of WRT and photodegradation on lateral exchanges between the**

397 **Congo River and its tributaries.** The lateral mixing between the central water masses

398    of the Congo River and DOM-rich water from the Cuvette Centrale was likely reduced

399    during FW due a greater photodegradation of terrestrial DOM. The downstream evolution

400    of $\delta^{13}C_{DOC}$ showed indeed that the lateral mixing between the mainstem and its tributaries

401    was strong during HW (Fig. 3c), but limited at FW during which $\delta^{13}C_{DOC}$ in the Congo

402    remained ~3 – 4 ‰ higher than values recorded in tributaries from km ~ 1600 to ~ 600

403    (Fig. 3d) despite slight increase in DOC concentrations (Fig. 3b). Photodegradation has

404    been assumed to be a major pathway to remove terrigenous DOM from aquatic

405    ecosystems (Cory et al., 2014) and mainly acts on colored, photosensitive molecules

406    associated with high MW and aromaticity (Spencer et al., 2009; Cawley et al., 2012;

407    Lapierre and del Giorgio, 2014). Greater photodegradation of DOM during FW was

408    supported by several lines of evidence. %C1 and %C3, both associated with highly

409    aromatic molecules (Table 2), were lower during FW compared to HW, and this decrease

410    occurred along with a decrease in DOM aromaticity (lower $SUVA_{254}$) and increase in

411    average MW (higher $S_R$) (Fig. 3 and 5). The more significant decrease in %C3 relative to

412    %C1 was also consistent with the well documented high photosensibility of this

413    component relative to other terrestrial humic-like component (Cawley et al., 2012; Lapierre

414    and del Giorgio, 2014). The role of DOM photodegradation in controlling the longitudinal

415    evolution of DOM in the Congo River during FW was also evidenced by the different

416    distribution of stations collected in the mainstem between HW (negative scores) and FW

417    (positive scores) along the PC2 of the PCA (Fig. 6).

418    Greater DOM photodegradation during FW implies a better exposure of CDOM to

419    sunlight irradiation, either spatially (i.e. in the water column) or temporally. The higher

420    coefficient of light attenuation in the water column ($K_d$) and associated lower Secchi

421    depths (Table 1) during FW indicates that the penetration of sunlight in the water column

422    was reduced compared to HW. This was likely due to the greater total suspended matter

423    (TSM) concentrations (Table 1) and phytoplanktonic development (Descy et al. 2016). It

424    is therefore more likely that the degree of DOM photodegradation was mainly driven by

425    changes in WRT. Decreasing water discharge and flow velocity during FW should lead to

426    an increase in WRT, allowing consequently more time for sunlight to degrade terrestrial

427    DOM.

428        The fact that %C4 was opposite to %C1 and %C3 along PC2 could either indicate

429    a photoproduction of this component (Massicotte and Frenette, 2011) or could simply

430    result from the fact that this component has been identify as photo-resistant to sunlight

431    irradiation (Ishii and Boyer, 2012). The longitudinal enrichment in %C4 reported during

432    HW along the mainstem rather advocate for a terrestrial origin from wetland areas. This

433    assumption is consistent with a recent study carried out in the Zambezi basin showing

434    that wetland areas exported greater proportion of similar C4 component towards river

435    channels relative to other terrestrial humic-like component during high flow periods

436    (Lambert et al., 2016).

437    **4.1.3. Role of large tributaries and channel width in controlling the longitudinal**

438    **evolution of DOM from Kisangani to Kinshasa.** DOM enrichment was more

439    pronounced within the core of the Cuvette Centrale (Fig. 2) that corresponds to the region

440    where the major tributaries of the Congo in terms of discharge (i.e. the Lulonga, the Ruki,

441    the Sangha, the Oubangui and the Kwa/Kasai rivers) connect the mainstem after receiving

442    great inputs of terrestrial DOM from the large flooded forest (Coynel et al., 2005; Laraque

443    et al., 2009) (Fig. 1 and Supplementary Fig. 1). DOC concentrations in the mainstem

444    increased faster immediately as the Congo enters in this central part of the Cuvette

445    Centrale during HW, reflecting the strong lateral mixing between water masses. However,

446    the net rise in DOC concentrations during FW were found to occurred first at ~70 km

447    downstream of the confluence zone with the Oubangui River, coinciding with a strong

448    reduction of the channel width (Supplementary Fig. 3). The ~1 ‰ drop in $\delta^{13}C_{DOC}$

449    associated with changes in DOM composition (especially increase in $SUVA_{254}$ and %C3)

450    at this station evidenced that the reduction of channel width favors the lateral mixing

451    between the mainstem and waters from the Cuvette Centrale that have traveled along the

452    river ridge lined by dense forest without being significantly impacted by photodegradation

453    (Supplementary Fig. 4). In fact, a "complete" lateral mixing with waters from the Cuvette

454    Centrale likely occurs only at the confluence zone with the Kwa/Kasai River. The high

455    dicharge of this tributary combined with a narrow channel width of the mainstem in this

456    part of the basin devoid of sand bars and islands (Runge et al., 2008) likely force lateral

457    exchanges. This is supported by the fact that $\delta^{13}C_{DOC}$ signatures of the Congo mainstem

458    became typical of black waters from the Cuvette Centrale only after connecting with the

459    Kwa/Kasai during FW, and could also explain why DOC increase is greater at this point

460    while DOC are largely higher in tributaries located upstream (e.g. The Ruki River).

461         Large tributaries also controlled the general evolution of DOM composition from

462    Kisangani to Kinshasa. Thus, DOM aromaticity ($SUVA_{254}$) decreased slightly along the

463    transect during HW (from ~4.6 to 4.2 mgC $L^{-1}$ $m^{-1}$ from Kisangani to Kinshasa), but

464    increased significantly during FW (from ~4.0 to 5.3 mgC $L^{-1}$ $m^{-1}$ from Kisangani to

465    Kinshasa) due to an increase in DOM aromaticity in large tributaries flowing through or

466    connected to the Cuvette Centrale.

467    **4.2. DOM transformation during its downstream transport in the Congo River**

468    **network.** Strahler stream order was used as an organizing concept for characterizing

469    individual stream reaches within the network (Strahler, 1957, Poole, 2010), and

470    investigate DOM composition across a gradient of streams and rivers. The loadings plot

471    along PC1 (Fig. 6) indicates a transition in the dominant DOM composition from aromatic

472    (%C3, $SUVA_{254}$) to aliphatic (%C2, %C6, FI) compounds. It is noteworthy that a similar

473    gradient in DOM composition has recently been reported in high-latitude lakes (Kellerman

474    et al., 2015) and in U.S. rivers networks (Creed et al., 2015), suggesting that the large-

475    scale governing processes controlling DOM in freshwater are similar across biomes.

476    However, the underlying mechanisms remain to be elucidated. Thus, the gain in aliphatic

477    DOM has been attributed to the increasing influence of autochthonous sources (Creed et

478    al., 2015) or to the degradation of terrestrial DOM (Kellerman et al., 2015), and external

479    factors (i.e. not related to DOM composition) have been suggested to have little influence

480    on this pattern (Kellerman et al., 2015). Our study supports the hypothesis that the

481    degradation of terrestrial DOM is the main driver on DOM transformation in aquatic

482    systems, but also highlights the role of landscape morphology and environmental

483    conditions in mitigating the transition from an aromatic to an aliphatic dominant

484    composition.

485    **4.2.1. Losses of aromatic DOM through photodegradation and biological activity as**

486    **producer of aliphatic DOM.** The preferential losses of aromatic molecules through

487    terrestrial DOM photodegradation was evidenced by the longitudinal evolution of DOM

488    along the mainstem during FW. Besides resulting in the removal of terrigenous DOM from

489    the river network, photodegradation was found to have a direct impact on the aquatic

490    metabolism in the Congo Basin. Indeed, %C5 was inversely correlated with (1) %C3 and

491    (2) measurements of pelagic community respiration (R) performed concurrently with DOM

492    sampling (Borges et al., 2015a) and attributed to bacterial respiration since phytoplankton

Biogeosciences
Discussions

Open Access
EGU

493     biomass is generally low (Descy et al. 2016) (Fig. 7). These relationships suggest that C5

494     was a direct photoproduct of terrestrial aromatic molecules tracked by C3 and that the

495     photoproduced organic molecules served as substrate for bacterial growth. This

496     assumption was supported by an experimental study showing that the formation of

497     component similar to C5 in boreal freshwaters was mediated by photodegradation

498     (Lapierre and del Giorgio, 2014) and is consistent with experiments claiming that the

499     aromatic and high MW fraction of terrestrial DOM can be photochemically converted into

500     more labile substances of lower MW that support the aquatic bacterial metabolism (Bano

501     et al., 1998; Tranvik and Bertilsson, 2001; Remington et al., 2011; Cory et al., 2014). The

502     lack of correlation between %C5 and R in the mainstem likely indicates an additional

503     source for labile DOM. The higher concentration of chlorophyll-a in the mainstem

504     compared to tributaries (Table 1) suggests that this source could be phytoplanktonic

505     exudation (Baines and Pace, 1991). Indeed, phytoplankton exudates have been shown to

506     be very labile and rapidly assimilated by bacteria in tropical lake waters (Morana et al.,

507     2014).

508           The gain in aliphatic DOM can be explained by the microbial reworking of terrestrial

509     DOM during its transport. Indeed, several studies carried out in a large variety of aquatic

510     ecosystems have attributed the origin of C2 and C6 to the biological degradation of

511     terrestrial DOM (Stedmon et al., 2003; Yamshita et al., 2010; Walker et al., 2013; Fasching

512     et al., 2014; Kellerman et al., 2015). The fact that %C2 and %C6 remained systematically

513     higher in the mainstem along the Kisangani – Kinshasa transect and did not decreased to

514     level similar to that of the tributaries strongly advocate for an internal production of these

515     components. This was supported by the higher FI values in the mainstem, indicating

516     greater inputs of microbially derived DOM in the Congo River compared to tributaries

517  (McKnight et al., 2001). Additionally, none of these components were correlated to

518  chlorophyll-a concentration (data not shown), suggesting that the phytoplankton primary

519  productivity in the Congo basin was not controlling their distribution contrary to what was

520  suggested in U.S. rivers (Creed et al., 2015). The dual role of microorganisms as

521  consumers of terrigenous DOM and producers of novel compounds has recently been

522  emphasized in DOM-rich black waters (Ward et al., 2013; Fasching et al., 2014).

523  It should be noted that previous investigations based on lignin biomarkers have

524  suggested that DOM transformation during transport in the Congo basin was mainly driven

525  by dynamic exchanges with the particulate organic carbon (POC) pool via sorption or

526  leaching processes (Spencer et al., 2012; Mann et al., 2014). This assumption was

527  however not supported by the weak relationship observed between $\delta^{13}C_{DOC}$ and $\delta^{13}C$ of

528  POC (Pearson's r = 0.20, *n* = 158, data not shown), suggesting limited exchange between

529  DOC and POC pools.

530  **4.2.2. External drivers on the aromatic towards aliphatic transition.** The enrichment

531  of the mainstem in the aliphatic fraction compared to the majority of its tributaries

532  advocates for a transition occurring during the downstream DOM transport in the fluvial

533  network. However, the large heterogeneity in the distribution of tributaries for a given

534  Strahler order indicates that landscape morphology and environmental properties can

535  mitigate downstream DOM transformation. Thus, DOM photodegradation is likely more

536  pronounced in catchments with large open areas, as suggested by the lower %C3 in

537  savannah-dominated catchments compared to forest-dominated catchments

538  (Supplementary Fig. 5, see also Lambert et al., 2015). Also, a strong connectivity with

539  terrestrial sources can maintain a greater aromatic character to DOM independently of the

540  size of the rivers. This typically refers to the well-known role of wetland areas in delivering

541  great quantity of aromatic DOM in inland waters (Hanley et al., 2013; Mann et al., 2014;

542  Lambert et al., 2016) and was illustrated by the comparison of DOM biogeochemistry in

543  the Oubangui River before and after it crosses the Cuvette Centrale. A multi-year

544  monitoring carried out at Bangui (Fig. 1) has indeed illustrated that the Oubangui

545  transported DOM of low aromaticity at the beginning of its rising water period occurring in

546  June (Bouillon et al., 2014) while our study reports highly aromatic DOM for the same

547  period. Finally, DOM bacterial degradation is likely limited in very acidic environments

548  (Borges et al., 2015a). This assumption is supported by the fact that %C2 and %C6 were

549  positively correlated with the pH of stream waters (Fig. 8). Such streams and rivers

550  typically correspond to the DOM-rich so-called "black-waters" originating from the Cuvette

551  Centrale, with pH between 3.6 and 5.9 and average 4.4 (Supplementary Fig. 6).

552  **4.3. The chemostat hypothesis and the pulse-shunt concept.** The chemostat

553  hypothesis suggests a decreasing of DOC concentrations and a convergence in DOM

554  composition towards lower aromaticity with increasing stream order because of the

555  increasing influence of in-stream processes that overwhelm terrestrial inputs from

556  headwater catchments (Creed et al., 2015). The shift from dominant terrestrial influence

557  to biogeochemical processing – assessed by the variation of $SUVA_{254}$ as a function of

558  stream order – has been estimated to occur in third- or fourth-order streams in river

559  networks across the United States (Creed et al., 2015). A net decrease in $SUVA_{254}$

560  associated with a decrease with DOC concentrations was only found to occur from six to

561  height order streams in our study (Fig. 9), reflecting the influence of the Cuvette Centrale

562  (i.e. strong connectivity with the flooded dense forest, acidic waters) on DOM

563  biogeochemistry in the Congo Basin. This falls in line with the "flood pulse concept" that

564  highlights the critical importance of the river-floodplain connectivity in lowland tropical

565 rivers such as the Amazon (Junk et al. 1989), while the chemostat hypothesis builds on

566 the river continuum concept (Vannote et al. 1980) that is typically applicable to rivers at

567 temperate latitudes (devoid on large wetlands). Also, an increase in DOM content and

568 aromaticity was found to occur at nine order streams, reflecting the fact that DOM-rich

569 waters from the Cuvette Centrale can travel along the ridge of the Congo River without

570 mixing totally with the central water masses of the mainstem (Supplemental Figure 4).

571 Overall, these observations illustrate how landscape properties can impact the functioning

572 of river ecosystems on DOM downstream transformation in river networks.

573 Our study also supports the "pulse-shunt" conceptual model that states that the

574 removal of terrestrial DOM in fluvial networks is a function of the hydrological regime of

575 the basin (Raymond et al., 2016). It should be noted that the seasonal variation in water

576 discharge is relatively low in the Congo Basin compared to other large rivers (Runge,

577 2008), but however enough to significantly impacts DOM photodegradation between FW

578 and HW. The switch between active and passive pipes is likely to be more pronounced in

579 large drainage basins in northern and southern Hemisphere with more contrasted

580 hydrological regimes, as recently showed in the adjacent Zambezi Basin (Lambert et al.,

581 2016). Our results also suggest that the photodegradation pathway is more sensitive to

582 changes in WRT compared to the biological pathway, but this hypothesis needs to be

583 verified in other environments.

584

585

586 **Data availability**

**Biogeosciences** Open Access
Discussions
EGU

587 The digital elevation model HydroSHEDS (Lehner et al., 2008) is available at

588 http://hydrosheds.cr.usgs.gov/index.php. The Global Lakes and Wetlands database

589 (Lehner and Döll, 2004) is available at http://www.worldwildlife.org/pages/global-lakes-

590 and-wetlands-database. The Global Land Cover 2009 database is available at

591 http://landcover.usgs.gov/landcoverdata.php.

604 **Author Contributions**

605 A.V.B., F.D., S.B. designed the study; A.V.B., and F.D. collected the field data; S.B. and

606 T.L. performed sample analysis; T.L. carried out the geographical system information

607 (GIS) analysis and performed the PARAFAC model with help of P.M.; T.L. analyzed the

608 data and drafted the manuscript that was revised and approved by all co-authors.

609 **References**

Biogeosciences
Open Access
Discussions
EGU

610  Baines, S. B. and Pace, M. L.: The production of dissolved organic matter by

611  phytoplankton and its importance to bacteria: patterns across marine and freshwater

612  systems, Limnol. Oceanogr., 36, 1078–1090, 1991.

613  Bano, N., Moran, M. A., and Hodson, R. E.: Photochemical formation of labile organic

614  matter from two components of dissolved organic carbon in a freshwater wetland,

615  Aquat. Microb. Ecol., 16, 95–102, 1998.

616  Battin, T. J., Kaplan, L. A., Findlay, S., Hopkinson, C. S., Marti, E., Packman, A. I.,

617  Newbold, J. D., and Sabater, F.: Biophys- ical controls on organic carbon fluxes in

618  fluvial networks, Nat. Geosci., 1, 95–100, 2008.

619  Battin, T. J.: Dissolved organic matter and its optical properties in a blackwater tributary

620  of the upper Oricono river, Venezuela, Org. Geochem., 28, 561-569,1998.

621  Berggren, M., Lapierre, J.-F., and del Giorgio, P. A.: Magni- tude and regulation of

622  bacterioplankton respiratory quotient across freshwater environmental gradients,

623  ISME J., 6, 984–993, doi:10.1038/ismej.2011.157, 2012.

624  Besemer, K., Luef, B., Preiner, S., Eichberger, B., Agis, M., and Peduzzi, P.: Sources and

625  composition of organic matter for bacterial growth in a large European river

626  floodplain system (Danube, Austria), Org. Geochem., 40, 321–331, 2009.

627  Bontemps, S., Defourney, P., Van Bogaert, E., and Arino, O.: GLOBCOVER2009

628  Products Description and Validation Report. (ESA and UCLouvain) (available online

629  at    http://ionia1.esrin.esa.int/docs/GLOBCOVER2009_Validation_Report_2.2.pdf),

630  2010 (Accessed: 15 September 2015).

631  Borcard, D., Gillet, F., and Legendre, P.: Numerical ecology with R, Springer New York,

632  New York, 306 pp., doi.org/10.1007/978-1-4419-7976-6, 2011.

633    Borges, A. V., Darchambeau, F., Teodoru, C. R., Marwick, T. R., Tamooh, F., Geeraert,

634        N., Omengo, F. O., Guerin, F., Lambert, T., Morana, C., Okuku, E., and Bouillon, S.:

635        Globally significant greenhouse-gas emissions from African inland waters, Nature

636        Geosci., 8, 637-642, doi:10.1038/ngeo2486, 2015a.

637    Borges, A. V., Abril, G., Darchambeau, F., Teodoru, C. R., Deborde, J., Vidal, L. O.,

638        Lambert, T., and Bouillon, S.: Divergent biophysical controls of aquatic $CO_2$ and $CH_4$

639        in the World's two largest rivers; Sci. Rep., 5, 15614, doi: 10.1038/srep15614, 2015b.

640    Bouillon, S., Yambélé, A., Gillikin, D. P., Teodoru, C. R., Darchambeau, F., Lambert, T.,

641        and Borges, A. V.: Contrasting biogeochemical characteristics of the Oubangui River

642        and tributaries (Congo River basin), Sci. Rep., 4, 1–10, doi:10.1038/srep05402,

643        2014.

644    Bouillon, S., Yambélé, A., Spencer, R. G. M., Gillikin, D. P., Hernes, P. J., Six, J., Merckx,

645        R., and Borges, A.V.: Organic matter sources, fluxes and greenhouse gas exchange

646        in the Oubangui River (Congo River basin), Biogeosciences, 9, 2045–2062,

647        doi:10.5194/bg-9-2045-2012, 2012.

648    Bricquet, J. P. : Les écoulements du Congo à Brazzaville et la spatialisation des apports,

649        in Grands Bassins Fluviaux Péri-atlantiques, edited by J. C. Olivry and J. Boulègue,

650        pp. 27–38, Inst. Fr. de Rech. Sci.pour le Dev. en Coop. (ORSTOM), Paris, 1995.

651    Bwangoy, J.-R. B., Hansen, M. C., Roy, D. P., De Grandi, G. and Justice, C. O.: Wetland

652        mapping in the Congo Basin using optical and radar remotely sensed data and

653        derived topographical indices, Remote Sens. Environ., 114, 73–86, 2010.

654    Cawley, K. M., Wolski, P., Mladenov, N., and Jaffé, R.: Dissolved organic matter

655        biogeochemistry along a transect of the Okavango delta, Bostwana, Wetlands, 32,

656        475–486, doi: 10.1007/s13157-012-0281-0, 2012.

Biogeosciences

Discussions

Open Access

EGU

657   Coble, P. G., Lead, J., Baker, A., Reynolds, D. M., and Spencer, R. G. M.: Aquatic Organic

658       Matter Fluorescence, NY: Cambridge University Press, New York, 375 pp., 2014.

659   Cole, J. J., Prairie, Y. T., Caraco, N. F., McDowell, W. H., Tranvik, L. J., Striegl, R. G.,

660       Duarte, C. M., Kortelainen, P., Downing, J. A., Middelburg, J. J., and Melack, J.:

661       Plumbing the global carbon cycle: integrating inland waters into the terrestrial carbon

662       budget, Ecosystems, 10, 171–184, 2007.

663   Cory, R. M., Harrold, K. H., Neilson, B. T., and King, G. W.: Controls on dissolved organic

664       matter (DOM) degradation in a headwater stream: the influence of photochemical

665       and hydrological conditions in determining light-limitation or substrate-limitation of

666       photo-degradation, Biogeosciences, 12, 6669-6685, doi:10.5194/bg-12-6669-2015,

667       2015.

668   Cory, R. M., McKnight, D. M., Chin, Y. P., Miller, P., and Jaros, C. L.: Chemical

669       characteristics of fulvic acids from Arctic surface waters: Microbial contributions and

670       photochemical transformations, J. Geophys. Res.-Biogeosci., 112, G04S51,

671       doi:10.1029/2006JG000343, 2007.

672   Cory, R. M., Ward, C. P., Crump, B. C., and Kling, G. W.: Sunlight controls water column

673       processing of carbon in arctic freshwaters, Science, 345, 925–928,

674       doi:10.1126/science.1253119, 2014.

675   Coynel, A., Seyler, P., Etcheber, H., Meybeck, M., and Orange, D.: Spatial and seasonal

676       dynamics of total suspended sediment and organic carbon species in the Congo

677       River, Global Biogeochem. Cy., 19, GB4019, doi:10.1029/2004GB002335, 2005.

678   Creed, I. F., McKnight, D., Pellerin, B. A., Green, M. B., Bergamaschi, B. A., Aiken, G. R.,

679       Burns, D. A., Findlay, S. E. G., Shanley, J. B., Striegl, R. G., Aulenbach, B. T., Clow,

680       D. W., Laudon, H., McGlynn, B. L., McGuire, K. J., Smith, T. A., and Stackpoole, S.

681    M.: The river as a chemostat: fresh perspectives on dissolved organic matter flowing

682    down the river continuum, Can. J. Fish. Aquat. Sci., 72, 1272–1285,

683    dx.doi.org/10.1139/cjfas-2014-0400, 2015.

684  Descy, J.P., Darchambeau, F., Lambert, T., Stoyneva, M.P., Bouillon, S., and Borges,

685    A.V.: Phytoplankton dynamics in the Congo River, submitted.

686  Fasching, C., Behounek, B., Singer, G. A., and Battin, T. J.: Microbial degradation of

687    terrigenous dissolved organic matter and potential consequences for carbon cycling

688    in brown-water streams, Scientific reports, 4, doi:10.1038/srep04981, 2014.

689  Fellman, J. B., Hood, E., and Spencer, R. G. M.: Fluorescence spectroscopy opens new

690    windows into dissolved organic matter dynamics in freshwater ecosystems: A

691    review, Limnol. Oceanogr., 55, 2452–2462, doi:10.4319/lo.2010.55.6.2452, 2010.

692  Hanley, K., Wollheim, W. M., Salisbury, J., Huntington, T., and Aiken, G.: Controls on

693    dissolved organic carbon quantity and chemical character in temperate rivers of

694    North America, Global Biogeochem. Cy., 27, 492–504, doi:10.1002/gbc.20044,

695    2013.

696  Helms, J. R., Stubbins, A., Ritchie, J. D., Minor, E. C., Kieber, D. J., and Mopper, K.:

697    Absorption spectral slopes and slope ratios as indicators of molecular weight,

698    source, and photobleaching of chromophoric dissolved organic matter, Limnol.

699    Oceanogr., 53, 955–969, 2008.

700  Ishii, S. K. L. and Boyer, T. H.: Behavior of reoccurring parafac components in fluorescent

701    dissolved organic matter in natural and engineered systems: A critical review,

702    Environ. Sci. Tech- nol. 46, 2006–2017, doi:10.1021/es2043504, 2012.

703  Junk, W., Bayley, P. B., and Sparks, R. E.: The flood pulse concept in river-floodplain

704    systems, Can. Spec. Publ. Fish. Aquat. Sci., 106, 110–127, 1989.

705 Kellerman, A. M., Kothawala, D. N., Dittmar, T., and Tranvik, L. J.: Persistence of

706      dissolved organic matter in lakes related to its molecular characteristics, Nat.

707      Geosci., 8, 454–457, doi: 10.1038/ngeo2440, 2015.

708 Kothawala, D. N., Stedmon, C. A., Müller, R. A., Weyhenmeyer, G. A., Köhler, S. J., and

709      Tranvik, L. J.: Controls of dissolved organic matter quality: Evidence from a large-

710      scale boreal lake survey, Glob. Change Biol., 20, 1101–1114,

711      doi:10.1111/gcb.12488, 2014.

712 Lambert, T., Pierson-Wickmann, A.-C., Gruau, G., Thibault, J. N., and Jaffrezic, A.:

713      Carbon isotopes as tracers of dissolved organic carbon sources and water pathways

714      in headwater catchments, J. Hydrol., 402, 228–238,

715      doi:10.1016/j.jhydrol.2011.03.014, 2011.

716 Lambert, T., Darchambeau, F., Bouillon, S., Alhou, B., Mbega, J- D, Teodoru, C. R., Nyoni,

717      F. C., Massicotte, P., and A V Borges, A. V.: Landscape control on the spatial and

718      temporal variability of chromophoric dissolved organic matter and dissolved organic

719      carbon in large African rivers, Ecosystems, 18, 1224–1239, doi:10.1007/s10021-

720      015-9894-5, 2015.

721 Lambert, T., Teodoru, C. R., Nyoni, F., Bouillon, S., Darchambeau, F., Massicotte, P., and

722      Borges, A. V.: Along-stream transport and transformation of dissolved organic matter

723      in a large tropical river, Biogeosciences, 13, 1–15, doi:10.5194/bg-13-1-2016, 2016.

724 Lapierre, J. F. and del Giorgio, P.A.: Partial coupling and differential regulation of

725      biologically and photochemically labile dissolved organic carbon across boreal

726      aquatic networks, Biogeosciences, 11, 5969–5985, doi:10.5194/bg-11-5969-2014,

727      2014.

Biogeosciences
Discussions

Open Access

EGU

728  Laraque, A., Bricquet, J. P., Pandi, A., and Olivry, J. C.: A review of material transport by

729      the Congo River and its tributaries, Hydrol. Process., 23, 3216–3224, 2009.

730  Leenheer, J. and Croué, J.: Characterizing aquatic dissolved organic matter, Environ. Sci.

731      Technol., 37, 18 – 26, 2003.

732  Lehner, B. and Döll, P.: Development and validation of a global database of lakes,

733      reservoirs and wetlands, J. Hydrol., 296, 1–22, doi:10.1016/j.jhydrol.2004.03.028,

734      2004.

735  Lehner, B., Verdin, K., and Jarvis, A.: New global hydrography derived from space borne

736      elevation data, Eos, 89, 93–94, 2008.

737  Ludwig, W., Probst, J.L., and Kempe, S.: Predicting the oceanic input of organic carbon

738      by continental erosion, Global Biogeochem. Cy., 10, 23-41, 1996.

739  Mann, P.J., Spencer, R. G. M., Dinga, B. J., Poulsen, J.R., Hernes, P.J., Fiske, G., Salter,

740      M. E., Wang, Z. A., Hoering, K.A., Six, J., and Holmes, R. M.: The biogeochemistry

741      of carbon across a gradient of streams and rivers within the Congo Basin. J.

742      Geophys. Res.-Biogeo., 119, 687–702, 2014.

743  Marín-Spiotta, E., Gruley, K. E., Crawford, J., Atkinson, E. E., Miesel, J. R., Greene, S.,

744      Cardona-Correa, C., and Spencer, R. G. M.: Paradigm shifts in soil organic matter

745      research affect interpretations of aquatic carbon cycling: transcending disciplinary

746      and ecosystem boundaries, Biogeochemistry, 117, 279-297, doi: 10.1007/s10533-

747      013-9949-7, 2014.

748  Massicotte, P. and Frenette, J.-J.: Spatial connectivity in a large river system: resolving

749      the sources and fate of dissolved organic matter, Ecol. Appl., 21, 2600–2617, 2011.

750 McKnight, D. M., Boyer, E. W., Westerhoff, P. K., Doran, P. T., Kulbe, T., and Andersen,

751 D. T.: Spectrofluorometric characterization of dissolved organic matter for indication

752 of precursor organic material and aromaticity, Limnol. Oceanogr., 46, 38–48, 2001.

753 Meybeck, M.: Riverine transport of atmospheric carbon: source, global typology and

754 budget. Water, Air, and Soil Pollution, 70, 443–463, 1993.

755 Morana, C., Sarmento, H., Descy, J.-P., Gasol, J.M., Borges, A. V., Bouillon, S., and

756 Darchambeau, F.: Production of dissolved organic matter by phytoplankton and its

757 uptake by heterotrophic prokaryotes in large tropical lakes, Limnol. Oceanogr., 59,

758 1364 – 1375, 2014.

759 Murphy, K. R., Stedmon, C. A., Graeber, D. and Bro, R.: Fluorescence spectroscopy and

760 multi-way techniques. PARAFAC. Anal. Methods 5, 6557–6566, 2013.

761 Neff, J. C., Finlay, J. C., Zimov, S. A., Davydov, S. P., Car- rasco, J. J., Schuur, E. A. G.,

762 and Davydova, A. I.: Seasonal changes in the age and structure of dissolved organic

763 carbon in Siberian rivers and streams, Geophys. Res. Lett., 33, L23401,

764 doi:10.1029/2006GL028222, 2006.

765 Ohno, T.: Fluorescence inner-filtering correction for determining the humification index of

766 dissolved organic matter, Environ. Sci. Technol., 36, 742–746,

767 doi:10.1021/Es0155276, 2002.

768 Osburn, C.L., Retamal, L., and Vincent, W.F.: Photoreactivity of chromophoric dissolved

769 organic matter transported by the Mackenzie River to the Beaufort Sea. Mar. Chem.

770 115, 10–20, doi: 10.1016/j.marchem.2009.05.003, 2009.

771 Poole, G. C.: Stream hydrogeomorphology as a physical science basis for advances in

772 stream ecology, J. N. Am. Benthol. Soc., 29, 12–25, 2010.

Biogeosciences

Open Access

Discussions

EGU

773　Raymond, P. A., Saiers, J. E., and Sobczak W. V.: Hydrological and biogeochemical

774　　controls on watershed dissolved organic matter transport: pulse-shunt concept,

775　　Ecology, 97, 5–16, doi.org/10.1890/14-1684.1, 2016.

776　Remington, S., Krusche, A., and Richey, J.: Effects of DOM photochemistry on bacterial

777　　metabolism and $CO_2$ evasion during falling water in a humic and a whitewater river

778　　in the Brazilian Amazon, Biogeochemistry, 105, 185–200, doi: 10.1007/s10533-010-

779　　9565-8, 2011.

780　Richardson, D. C., Newbold, J. D., Aufdenkampe, A. K., Taylor, P. G., and Kaplan, L. A.:

781　　Measuring heterotrophic respiration rates of suspended particulate organic carbon

782　　from stream ecosystems, Limnol. Oceanogr.-Meth., 11, 247–261, 2013.

783　Runge, J.: The Congo River, Central Africa in Large Rivers: Geomorpholgy and

784　　Management, Ed. Gupta, A., John Wiley & Sons, Ltd, 293–309, 2008.

785　Sanderman, J., Lohse, K. A., Baldock, J. A., and Amundson, R.: Linking soils and streams:

786　　sources and chemistry of dissolved organic matter in a small coastal

787　　watershed,Water Resour. Res., 45, W03418, doi:10.129/2008WR006977, 2009.

788　Spencer, R. G. M., Stubbins, A., Hernes, P. J., Baker, A., Mopper, K., Aufdenkampe, A.

789　　K., Dyda, R. Y., Mwamba, V. L., Mangangu, A. M., Wabakanghanzi, J. N., and Six,

790　　J.: Photochemical degradation of dissolved organic matter and dissolved lignin

791　　phenols from the Congo River, J. Geophys. Res.-Biogeo., 114,

792　　doi:10.1029/2009jg000968, 2009.

793　Spencer, R. G. M., Hernes, P. J., Ruf, R., Baker, A., Dyda, R. Y., Stubbins, A., and Six,

794　　J.: Temporal controls on dissolved organic matter and lignin biogeochemistry in a

795　　pristine tropical river, Democratic Republic of Congo, J. Geophys. Res., 115,

796　　G03013, doi:10.1029/2009JG001180, 2010.

797   Spencer, R. G. M., Hernes, P. J., Aufdenkampe, A. K., Baker, A., Gulliver, P., Stubbins,

798       A., Aiken, G. R., Dyda, R. Y., Butler, K. D., Mwamba, V. L., Mangangu, A. M.,

799       Wabakanghanzi, J. N., and Six, J.: An initial investigation into the organic matter bio-

800       geochemistry of the Congo River, Geochim. Cosmochim. Acta, 84, 614–627, 2012.

801   Stedmon, C. A. and Markager, S.: Resolving the variability in DOM fluorescence in a

802       temperate estuary and its catchment unsing PARAFAC, Limnol.Oceanogr, 50, 686–

803       697, 2005.

804   Stedmon, C. A., Markager, S., and Bro, R.: Tracing dissolved organic matter in aquatic

805       environments using a new approach to fluorescence spectroscopy, Mar. Chem., 82,

806       239–254, doi:10.1016/s0304-4203(03)00072-0, 2003.

807   Strahler, A.N.: Quantitative analysis of watershed geomorphology, T. Am. Geophys.

808       Union, 38, 913–920, 1957.

809   Stubbins, A., Lapierre, J.F., Berggren, M., Prairie, Y.T., Dittmar, T., and del Giorgio, P.A.:

810       What's in an EEM? Molecular signatures associated with dissolved organic

811       fluorescence in boreal Canada, Environ Sci. Technol., 48, 10598–10606, 2014.

812   Tranvik, L. J. and Bertilsson, S.: Contrasting effects of solar UV radiation on dissolved

813       organic sources for bacterial growth, Ecol. Lett., 4, 458–463, 2001.

814   Vannote, R. L., Minshall, G. W., Cummins, K. W., Sedell, J. R., and Cushing, C. E.: The

815       river continuum concept, Can. J. Fish. Aquat. Sci., 37, 130–137, 1980.

816   Wagner, S., Jaffé , R., Cawley, K., Dittmar, T., and Stubbins, A.: Associations Between

817       the Molecular and Optical Properties of Dissolved Organic Matter in the Florida

818       Everglades, a Model Coastal Wetland System. Front. Chem. 3:66. doi:

819       10.3389/fchem.2015.00066, 2015.

820    Walker, S. A., Amon, R. M., and Stedmon, C. A.: Variations in high-latitude riverine

821        fluorescent dissolved organic matter: A comparison of large Arctic rivers, J.

822        Geosphys. Res-Biogeo., 118, 1689–1702, doi:10.1002/2013JG002320, 2013.

823    Ward, N. D., Keil, R. G., Medeiros, P. M., Brito, D. C., Cunha, A. C., Dittmar, T., Yager, P.

824        L., Krusche, A. V., and Richey, J. E.: Degradation of terrestrially derived

825        macromolecules in the Amazon River, Nat. Geosci., 6, 530–533,

826        doi:10.1038/ngeo1817, 2013.

827    Weishaar, J. L., Aiken, G. R., Bergamaschi, B. A., Fram, M. S., Fujii, R., and Mopper, K.:

828        Evaluation of specific ultraviolet absorbance as an indicator of the chemical

829        composition and reactivity of dissolved organic carbon, Environ. Sci. Technol., 37,

830        4702–4708, doi: 10.1021/es030360x, 2003.

831    Weyhenmeyer, G. A., Fröberg, M., Karltun, E., Khalili, M., Kothawala, D., Temnerud, J.,

832        and Tranvik, L. J.: Selective decay of terrestrial organic carbon during transport from

833        land to sea, Glob. Change Biol., 18, 349–355, doi:10.1111/j.1365-

834        2486.2011.02544.x, 2012.

835    Yamashita, Y., Scinto, L. J., Maie, N., and Jaffé, R.: Dissolved organic matter

836        characteristics across a subtropical wetland's landscape: application of optical

837        properties in the assessment of environmental dynamics, Ecosystems, 13, 1006–

838        1019, doi:10.1007/s10021-010-9370-1, 2010.

839    Zepp, R. G., Sheldon, W. M., and Moran, M. A.: Dissolved organic fluorophores in

840        southeastern US coastal waters: correction method for eliminating Rayleigh and

841        Raman scattering peaks in excitation–emission matrices, Mar. Chem., 89, 15–36,

842        doi:10.1016/j.marchem.2004.02.006, 2004.

**Figures captions**

**Figure 1 –** Maps of the Congo Basin showing (a) the elevation (Lehner et al., 2008), the main hydrological network, the extent of the Cuvette Centrale (Lehner and Döll, 2004), the distribution of sampling sites along the Kisangani – Kinshasa transect and (b) the dominant land cover (Bontemps et al., 2011). The red line "A" indicates the entrance of the Congo River within the core of the Cuvette Centrale (see text for details and supplementary figure 1).

**Figure 2 –** Average freshwater discharge of the Congo River at Kinshasa, and corresponding water height at the gauging station, for the period 2003-2013. Timing of the two cruises is indicated by thicker lines.

**Figure 3 –** Longitudinal evolution of DOM properties in the mainstem, large and small tributaries along the Kisangani-Kinshasa transect during HW (left panels) and FW (right panels). From top to bottom the panels represent: DOC, $\delta^{13}C_{DOC}$, $SUVA_{254}$, $S_R$ and FI. Numbers refer to large tributaries: (1) the Kwa/Kasai, (2) the Lefini, (3) the Sangha, (4) the Oubangui, (5) the Ruki, (6) the Ikelemba, (7) the Lulonga, (8) the Mongala, (9) the Itimbiri, (10) the Aruwini, (11) the Lomami, (12) the Lindi and (13) the Tshopo River.

**Figure 4 –** Relationships between DOC concentrations in tributaries and the extent of flooded dense forest.

**Figure 5 –** Longitudinal evolution of the relative contribution of PARAFAC component in the mainstem, large and small tributaries along the Kisangani-Kinshasa transect during HW (left panels) and FW (right panels).

**Figure 6 –** Graphical representation of PCA results, including loadings plot for the input variables and scores plot for stations based on (a) their Strahler stream order or (b) sampling location. PCA results based on the hydrological period is included in each plot.

Biogeosciences

Discussions

Open Access

EGU

867    **Figure 7 –** (a) Relationship between %C5 and %C3 and (b) relationships between %C5

868    and pelagic community respiration (R) in the Congo Basin.

869    **Figure 8 –** Relationship between the relative contribution of aliphatic components (C2 and

870    C6) and pH of stream waters in the Congo Basin.

871    **Figure 9 –** DOC concentrations and DOM aromaticity ($SUVA_{254}$) across a gradient of

872    streams and rivers in the Congo Basin as a function of stream order. The box spans the

873    interquartile range (25–75 percentiles), whiskers correspond to min-max values,

874    horizontal bar to median, cross to average.

875

**Table 1 –** Selected attributes (mean±standard deviation, min-max) of sampling sites

during the field campaigns: oxygen saturation level (%$O_2$), pH, Secchi depths, vertical

light attenuation coefficient ($K_d$), total suspended matter (TSM) and Chlorophyll-a

concentrations.

| Period | n | %$O_2$ (%) | pH | Secchi (cm) | $K_d$ ($m^{-1}$) | TSM (mg $L^{-1}$) | Chla (µg $L^{-1}$) |
|---|---|---|---|---|---|---|---|
| **Maximum high waters** | | | | | | | |
| Mainstream | 35 | 60.3±10.6 (48.4-89.2) | 6.46±0.22 (6.07-6.92) | 54.6±15.6 (25-80) | 1.54±0.37 (1.06-2.83) | 29.4±21.9 (14.0-99.8) | 0.84±0.42 (0.10-1.76) |
| Major tributaries | 13 | 54.3±33.3 (8.6-111.3) | 5.67±1.09 (3.91-6.87) | 79.5±60.7 (25-250) | 1.55±0.61 (0.44-2.46) | 12.5±13.3 (0.74-44.4) | 0.54±1.02 (0.01-3.57) |
| Minor tributaries | 26 | 27.9±30.2 (4.2-99.8) | 5.33±0.75 (3.91-6.17) | 86.2±29.7 (15-140) | 1.51±0.49 (0.89-2.79) | 7.7±13.4 (1.7-71.4) | 0.35±0.42 (0-1.85) |
| **Falling waters after second peak water discharge** | | | | | | | |
| Mainstream | 34 | 84.8±7.4 (54.2-93.4) | 6.82±0.32 (6.08-7.38) | 46.8±5.7 (35-62) | 3.86±0.58 (1.52-4.65) | 31.9±9.1 (4.0-45.4) | 3.99±1.54 (1.13-7.68) |
| Major tributaries | 12 | 62.1±31.2 (0.3-98.2) | 5.77±1.22 (3.63-7.05) | 66.7±23.4 (35-106) | 3.34±0.66 (2.44-5.09) | 14.4±12.5 (0.73-43.0) | 1.65±2.27 (0.017-6.39) |
| Minor tributaries | 41 | 37.8±35.6 (0.3-103.0) | 4.56±0.77 (3.6-6.1) | 80.7±42.2 (38-205) | 3.36±0.95 (1.48-5.16) | 6.1±6.5 (0.5-34.8) | 0.55±0.99 (0.009-5.12) |

880

881
882
883
884
885

**Table 2** – Spectral properties (excitation and emission maxima ($Ex_{max}$/$Em_{max}$)) of the six components identified using PARAFAC modelling, correspondence with peak classification, general assignment and comparison with previously identified components in different environments, dominant molecular association and possible source and reactivity. Dominant molecular association is based on FTICR-MS studies. Numbers in brackets refer to the second peak of maximal excitation.

| Component | $Ex_{max}$ (nm) | $Em_{max}$ (nm) | Peak(s) name[1] | General assignment[2] | Comparison with others environments | | | | | | | Dominant molecular association[4,6,10] | Potential sources and reactivity* |
|---|---|---|---|---|---|---|---|---|---|---|---|---|---|
| | | | | | Arctic Rivers[3] | St Lawrence River[4] | Boreal streams[5,6] | Boreal lakes[7,8] | Tropical wetland[8,10] | Zambezi basin[11] | Tropical wetland[12] | | |
| C1 | <260 (375) | 488 | A+/C+ | Terrestrial humic-like | C3 | C3 | C2 | C3 | C5 | C2 | C2 | High aromaticity, high MW | T[1-12], P[-5] |
| C2 | 305 (<260) | 414 | M | Microbial humic-like | — | C7 | C5 | C2 | C4 | C3 | C3 | Aliphatic, low MW | M+[8-10] |
| C3 | 330 (<260) | 444 | $A_c$/C | Terrestrial humic-like | C1 | C2 | C3 | C1 | C6 | C1 | C1 | High aromaticity, high MW | T[1-12], P[5,9,10] |
| C4 | <260 | 444 | $A_c$ | Terrestrial humic-like | — | C1 | — | C5 | C2 | C4 | — | Aromatic, intermediate MW | T[9-11], P+[4], Pr[-10] |
| C5 | 350 | 424 | C | Humic-like | — | — | C4 | — | — | — | — | Low aromaticity, low MW | P[5] |
| C6 | 275 | 350 | B/T | Tryptophan-like | C5 | C4 | C6 | C6 | C7 | C5 | C4 | Aliphatic, low MW | Au[4,9,11], M+[3,7], M-[5] |

(1) Coble et al., 2014; (2) Fellman et al., 2010; (3) Walker et al., 2013; (4) Massicotte and Frenette, 2011; (5) Lapierre and del Giorgio, 2014; (6) Stubbins et al., 2014 (FTICR-MS); (7) Kothawala et al., 2014; (8) Kellerman et al., 2015 (FTICR-MS); (9) Yamashita et al., 2010; (10) Cawley et al., 2012; (11) Lambert et al., 2016; (12) Wagner et al., 2015 (FTICR-MS)
*Au: autochtonous production; T: terrestrial inputs; M+: microbial dregradation; M-: biolabile; P+: photoproduct; Pr:photo-resistant; P-: photosensible

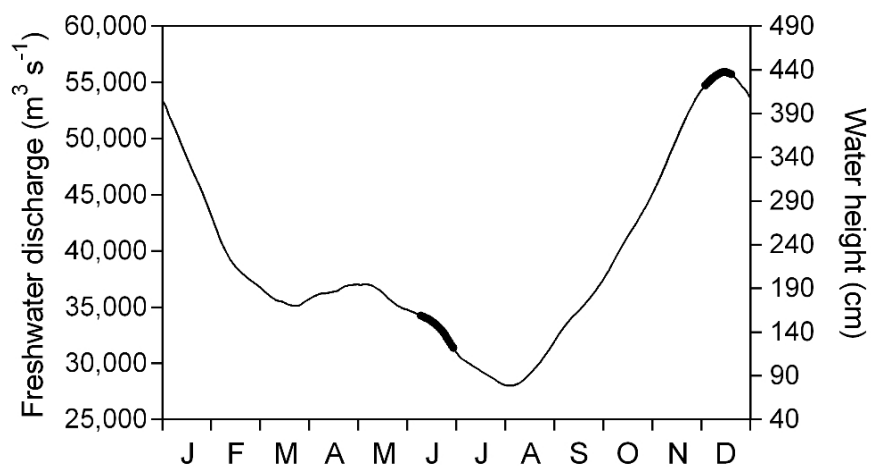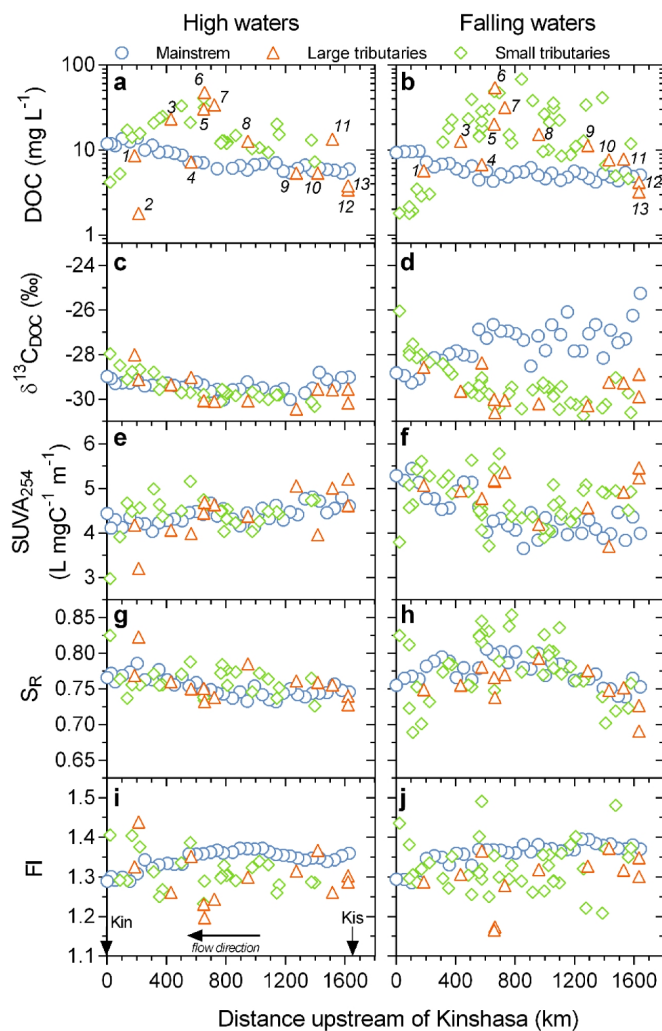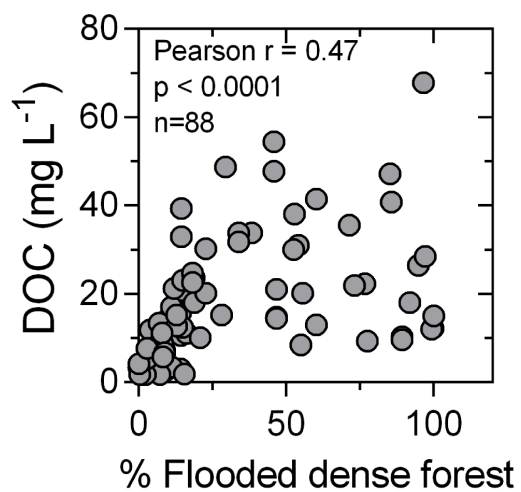886
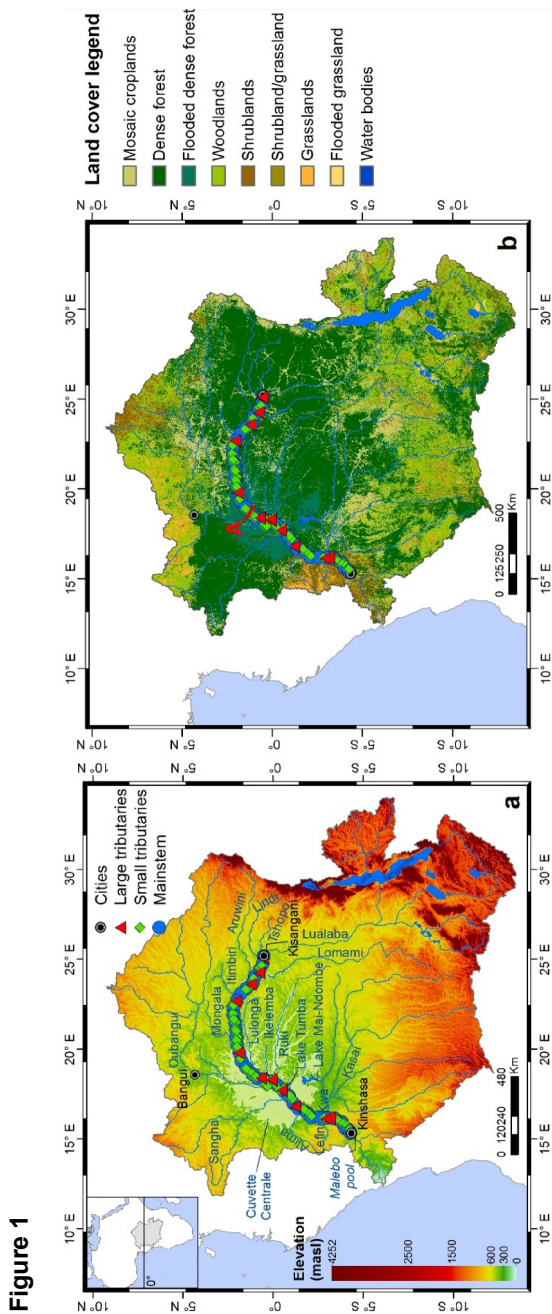
**Figure 1**

890     **Figure 2**



891

892 **Figure 3**

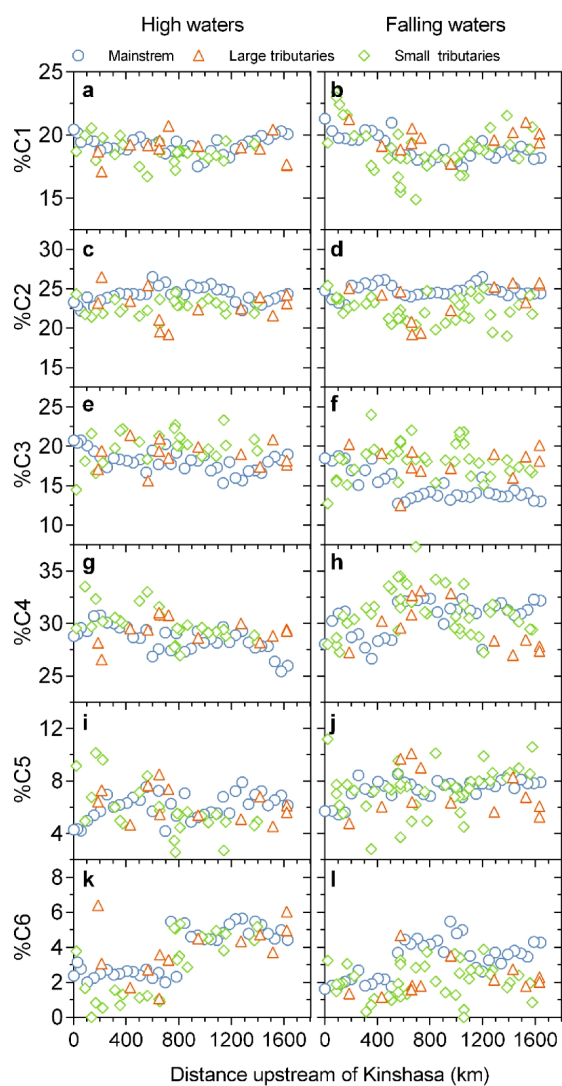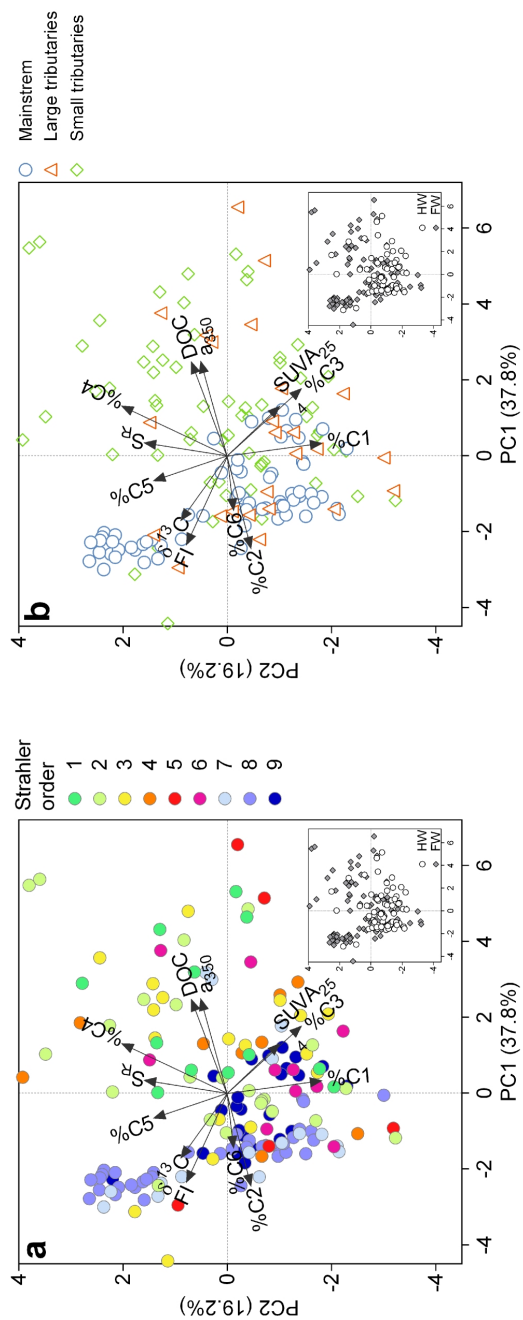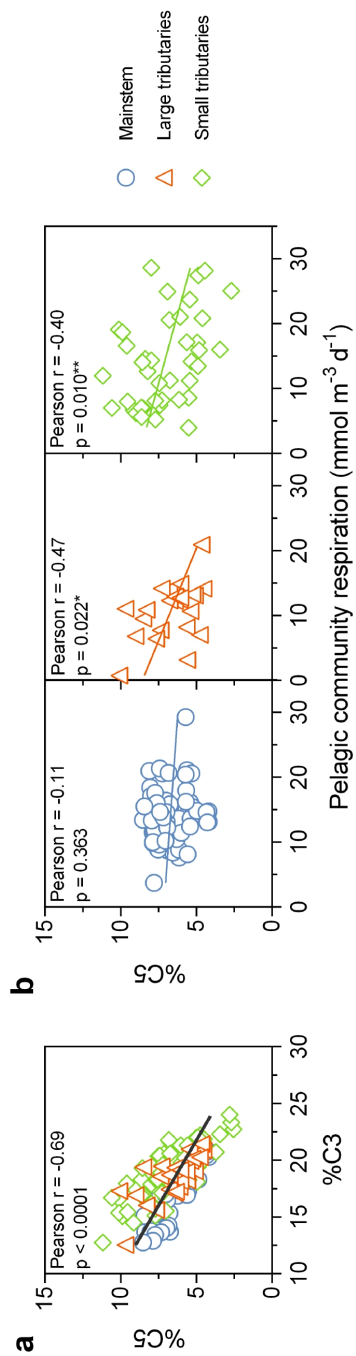

893

894    **Figure 4**
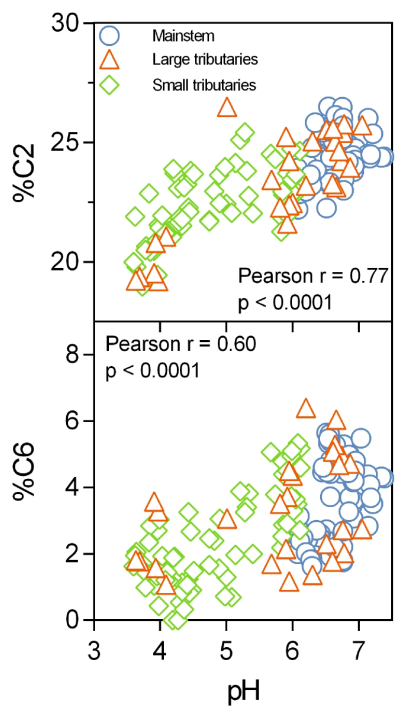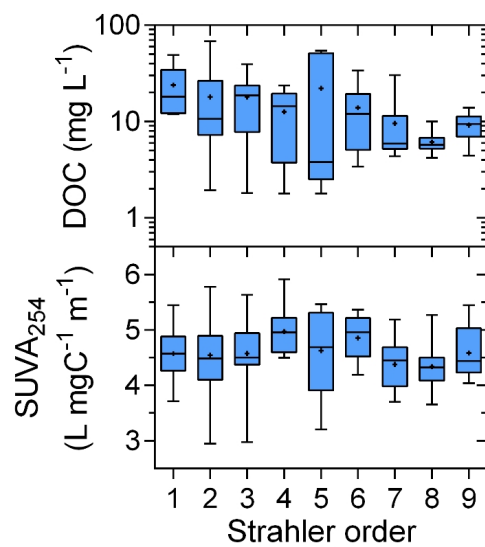


895

896    **Figure 5**



897

**Figure 6**

**Figure 7**



900

901

902    **Figure 8**



903

904  **Figure 9**



905